mater.scichina.com link.springer.com

Published online 24 April 2024 | https://doi.org/10.1007/s40843-024-2823-9
Sci China Mater 2024, 67(5): 1481–1490

Substrate-free ultra-thin epidermal bioelectrodes with enhanced conformality and breathability for long-term physiological monitoring

Guanjun Li[†], Yanting Gong[†], Shiqiang Fang, Tong You, Ruirui Shao, Lanqian Yao, Chen Liu, Chunjin Wu, Jian Niu[*] and Wen-Yong Lai[*]

ABSTRACT **The development of durable and reliable bioelectrodes for high-quality bioelectrical signals acquisition has become a crucial technology in the field of human physiological condition monitoring and human-machine interfaces. However, most existing bioelectrodes are limited to conventional elastomeric substrates that suffer from mechanical mismatch and low permeability, and lack multifaceted attributes and essential synergistic properties akin to those found in biological skins. In this work, we report advanced substrate-free ultra-thin epidermal bioelectrodes (ASU-EBEs) based on free-standing conductive all-polymer (FCAP) films, which integrate the advantages of ultra-conformality, excellent stretchability and breathability into a single device. The resulting ASU-EBEs exhibit excellent conductivity of ~475 S cm^{-1}, outstanding stretchability of ~48%, ultra-conformality to the interface of biological tissues and superior breathability. The enhanced electronic and mechanical performance is attributed to the introduction of water-soluble polyethylene oxide into poly(3,4-ethylenedioxythiophene): poly(4-styrenesulfonate) (PEDOT:PSS) to control the molecular π-π stacking distance and promote the formation of nanofiber structures. Hence, ASU-EBEs show much lower skin-contact impedance than the standard gel electrodes, enabling the use for long-term healthcare monitoring in complex daily conditions.**

Keywords: flexible bioelectronics, epidermal bioelectrodes, free-standing conductive films, conformality, breathability

INTRODUCTION

Epidermal bioelectronics refer to a class of advanced wearable devices that integrate with the skin in a manner that closely resembles the natural properties of the epidermis, with a wide range of applications in healthcare, diagnostics, and human-machine interfaces [1–4]. Bioelectrodes, as an essential component of wearable devices, are in direct contact with the skin and are capable of recording bioelectrical signals reliably over a long period of time through non-invasive monitoring [5]. Existing studies show that most biological tissues are three-dimensional (3D), soft, and stretchable, imposing high requirements on the design of bioelectrodes [4]. Bio-interfacial adaptability and long-term reliability are recognized as fundamental principles in the invention of optimal bioelectrodes [2,4]. These principles include several sub-principles, including excellent stretchability to ensure conformity with the dynamic surfaces of biological tissues, and excellent breathability to facilitate gas/nutrient exchange between biological tissues and the external environment [6–8]. The existing bioelectrodes consist mainly of gel electrodes (i.e., Ag/AgCl electrodes) that display high-quality signals [5,9,10]. However, these gel bioelectrodes are usually thick (>50 μm) and unable to form conformal contact with the skin, and are designed by molecular structure to impart adhesion, which requires complex synthetic steps [11]. Ultra-thin epidermal bioelectrodes, with a Young's modulus comparable to that of the skin, a thickness of less than 1 μm, and biocompatibility, are an ideal option for achieving low motion artifacts, high signal-to-noise ratios (SNRs), and stable monitoring of electrophysiological signals over time [12–14].

Currently, such epidermal bioelectrodes are typically fabricated on soft and thin substrates [15]. They must possess thinness and softness to ensure for seamless contact with undevelopable surfaces, as well as compatibility and adhesion to skin and organs. However, the presence of substrates covering restricts breathability and deformability, making it susceptible to motion artifacts [7]. Substrate-free ultra-thin epidermal bioelectrodes represent a novel approach to establish intimate contact between epidermal bioelectrodes and the skin. 2D materials (e.g., graphene, MXene, and MoS_2) can form free-standing films through interlayer van der Waals interactions, making them popular choices for fabricating subsrate-free, ultra-thin epidermal bioelectrodes [9,16–19]. The inherent limitations arising from the topological structure compromise conductivity and mechanical properties, consequently restricting their potential utilization in epidermal bioelectrodes [19]. In contrast, conductive polymers, such as poly(3,4-ethylenedioxythiophene): poly(4-styrenesulfonate) (PEDOT:PSS), offer promising potential for developing substrate-free, ultra-thin epidermal bioelectrodes due to their π–π stacking interactions among adjacent PEDOT chains and morphology modulation [20–22]. Despite efforts to enhance electrical conductivity and stretchability by incorporating ionic and molecular additives, challenges remain in terms of mechanical fragility, potential insufficiency in conductivity for high-precision applications, and susceptibility to chemical instability [20,23]. Moreover, breathable ultra-thin epidermal bioelectrodes using conducting polymers, especially

State Key Laboratory of Organic Electronics and Information Displays (SKLOEID), Institute of Advanced Materials (IAM), School of Chemistry and Life Sciences, Nanjing University of Posts & Telecommunications, Nanjing 210023, China

[†] These authors contributed equally to this work.

[*] Corresponding authors (emails: iamwylai@njupt.edu.cn (Lai WY); iamjniu@njupt.edu.cn (Niu J))

PEDOT:PSS, have not yet been reported. The development of advanced ultra-thin epidermal bioelectrodes based on conductive polymers that comply with the fundamental and sub-principles, including ultra-conformality, excellent stretchability and breathability is highly desirable yet remains unexplored.

Herein, we propose an effective strategy to develop an advanced substrate-free ultra-thin epidermal bioelectrode (ASU-EBE) for flexible bioelectronics based on a novel free-standing conductive all-polymer (FCAP) film by incorporating water-soluble polymer, polyethylene oxide (PEO), into rigid PEDOT:PSS composites. The introduction of PEO, which forms nanofiber structures due to their polar groups, facilitates the phase separation between PEDOT and PSS chains, thereby imparting the ASU-EBEs with integrated properties of electrical conductivity, breathability and stretchability. The ASU-EBEs achieve outstanding ultra-conformality due to their ultrathin nature and are able to adapt to the unique micro-tissues of human skin through van der Waals interactions. Moreover, it demonstrates remarkable stretchability with a strain capacity of 48%, significantly surpassing that of human skin (25%) [4]. Notably, these ASU-EBEs show excellent breathability with approximately seven times higher the typical percutaneous water loss rate [24], which represents the first example of breathable bioelectrodes based on PEDOT:PSS conductive polymers. As a result, bioelectrical signals including electrocardiogram (ECG) [25], electrooculography (EOG) [26], electromyogram (EMG) [18], and electroencephalogram (EEG) [27] have been successfully acquired using these ASU-EBEs, demonstrating their exceptional utility in complex situations. The development and application of these ASU-EBEs are critical to expanding the field of flexible bioelectronics.

EXPERIMENTAL SECTION

Materials

PEDOT:PSS (PH1000) aqueous solution was purchased from Heraeus. *N*,*N*-dimethylformamide (DMF) (anhydrous, 99.8%), poly(ethylene oxide) (average $M_w \approx 5{,}000{,}000$), PEO (average $M_w \approx 1{,}000{,}000$, $M_w \approx 8{,}000{,}000$, and $M_w \approx 2500$) was obtained from Sigma. Capstone^{TM} FS30 was purchased from Chemours. Polydimethylsiloxane (PDMS) precursors (SYLGARD 182) were purchased from Ellsworth Adhesives. All of the chemical reagents were used exactly as they were received, with no further purification.

Preparation of FCAP film

The experimental details, including preparation of PEDOT/PEO mixed solution and preparation of FCAP film, were described in the Supplementary information (SI).

Structures characterization

The methods used to characterize the mechanical and electrical properties, morphology, and structure of FCAP films were described in SI. In addition, specific testing of the air permeability of FCAP films and testing of electrophysiological signals as bioelectrodes are also described in SI.

RESULTS AND DISCUSSION

Preparation and characterization of FCAP films

The FCAP films were manufactured by introducing water-soluble polymer PEO into the PEDOT films (Fig. 1a, b). The detailed processing of the FCAP films can be found in the section of Methods in SI. PEDOT:PSS is a class of conducting polymers with intrinsic mechanical flexibility and a modulated condensed matter structure. Due to the limitations of the conjugated structures, their stretchability (approximately 5%) and conductivity (<2 S cm^{-1}) remain poor. Considering the advantages of PEO, such as its non-volatility, water solubility, and good miscibility, it was selected as an additive to improve the mechanical performance (mechanical strength and stretchability) and electrical conductivity of PEDOT films. The electrical conductivity and mechanical properties of the FCAP films were significantly affected by the amount and weight of PEO (Figs S1 and S2). In order to achieve a balance of performances among electrical conductivity, mechanical stretchability and optical transmittance, PEO with a molecular weight of 5,000,000 was chosen (Table S1).

As shown in Fig. 2a and Movie S1, the mechanical strength of the PEDOT films was substantially improved after the introduction of PEO. Continuous FCAP films can float easily on water, fold repetitively without breaking and suspend over open holes without rupturing (Fig. 2b). In contrast, the PEDOT films were fractured on the surface of the water (Fig. S3). It is well known that surface wettability is essential to ensuring efficient adhesion between bioelectrodes and biological tissues. It has been found that the PEDOT:PSS/PEO mixed solution exhibits excellent wettability on various substrates because of the presence of the –OH functional group in PEO, facilitating the formation of homogeneous and continuous films during the preparation process (Figs S4–S6). Additionally, the FCAP films also have better wettability (with a water contact angle of 20.1°) than the PEDOT films (water contact angle of 51.6°), which is advantageous for closely interacting with wet biological tissues (Fig. 2c). Rapid gas/nutrient exchange between tissues and the environment relies on breathability for bioelectronic applications. Thus, the water vapor transmission rate of FCAP films suspended over an open hole is 32 mg cm^{-2} h^{-1}, which is approximately seven times higher than the average transepidermal water loss (TEWL) rate (4.4 mg cm^{-2} h^{-1}) (Fig. 2d) [24]. The permeability of FCAP films was hypothesized to be related to the internal morphology, which was later confirmed.

Moreover, the mechanical stretchability of the FCAP films, such as the elongation at break and the Young's modulus, was also significantly enhanced by introducing PEO into the PEDOT films. FCAP films showed a linear stress-strain curve with tensile strains as high as 48% and a Young's modulus (90 MPa) more than an order of magnitude lower than that of PEDOT films (2.5 GPa) (Fig. 2e) [23]. Fig. 2g compares the electrical conductivity of FCAP films and PEDOT films. Since PEDOT films are unable to maintain macrostructural integrity in a free-standing form, measurements were performed on composite films combined with PDMS substrates. The relative resistance of the PEDOT films displays a slow linear rise up to 10% tensile strain and a sharp increase after 10%, indicating that the PEDOT films start to fracture macroscopically at strains above 10%. In contrast, FCAP films do not show a rapid rise in resistance until the tensile strain exceeds 40%. When the tensile strain exceeded 40%, their microcracks and conductive paths were significantly reduced (Fig. 2f). The adaptability and conformability of FCAP films to microscopic surface topographies were also investigated by scanning electron microscopy (SEM). FCAP films present

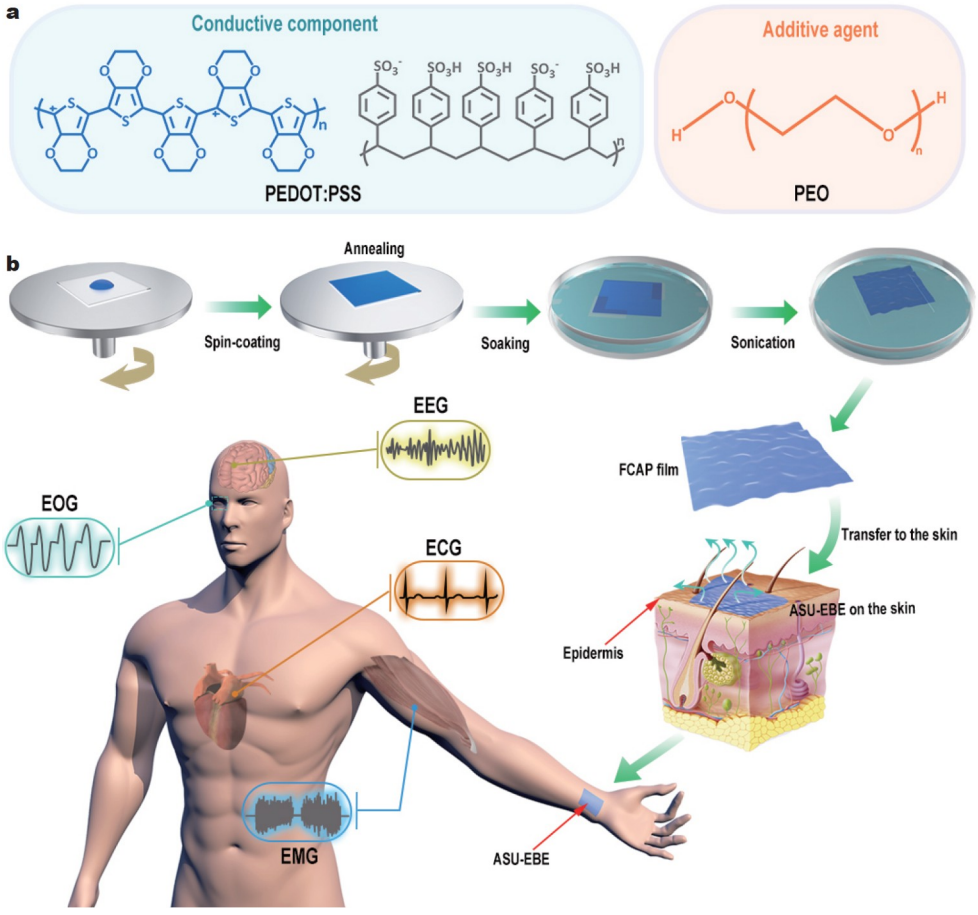

Figure 1 Fabrication schematic of the FCAP films. (a) Chemical structures of PEDOT:PSS and PEO. (b) Fabrication process of the FCAP films: first, PEDOT:PSS/PEO mixed solutions were spin-coated on glass substrates; second, the FCAP films were annealed and dried; third, they were subjected to mild sonication in a vessel filled with deionized water. The resulting FCAP films can be used as an ultra-conformal and breathable ASU-EBE for epidermal biopotential detection.

highly conformal interfaces with microsphere arrays (10 μm in diameter) (Fig. 2h and Fig. S8), including isolated individual microspheres and clusters of two or three microspheres (Fig. 2i), which conformally wrap around the microspheres without tearing. They can be easily transferred to the surface of complex biological tissues by "wet transfer" methods owing to their outstanding mechanical properties, creating a seamless fit for long-term and accurate monitoring of body health (Fig. S7 and Movie S2). As shown in Fig. 2j, k, the transferred FCAP films formed an ultra-conformal interface with perfect compliance, as confirmed by an optical microscopy.

To get further insight into the role of PEO, the stress-strain curves of FCAP films were measured as shown in Fig. 3a. It was observed that the FCAP film was obviously "softened" after being doped with PEO, exhibiting improved mechanical stretchability. The elongation at the break was reduced due to the formation of large crystallites with elevated PEO concentrations in FCAP films. Therefore, when the weight fraction of the doped PEO is 33 wt%, the maximum elongation at break of the FCAP film is 48%, which is significantly higher than that of the pure PEDOT film (3%) (Fig. 3b). These mechanical properties are similar to those of human tissues such as nerve tissue (20%), and skin (50%) [4]. In addition, the Young's modulus of FCAP films decreased from 269 to 80 MPa with the increase of the PEO contents from 0 to 33 wt% (Fig. 3b), which is equivalent to that of some soft elastomers. Furthermore, the conductivity of FCAP films shows a similar phenomenon (Fig. 3c). The maximum conductivity of FCAP film was further increased from 475 to 3204 S cm^{-1} after immersing the film in concentrated sulfuric acid. In addition, the prepared FCAP films have excellent bending stability, uniformity and wettability, and can be processed into complex flexible transparent circuit patterns by solution processing techniques (Fig. 3c, Figs S9, S10 and Movie S3).

Structure and morphology of FCAP films

Generally, excellent conductivity requires a stiff phase with strong crystallinity. In contrast, outstanding mechanical stretchability is usually associated with a soft amorphous phase and a high degree of chain-folding disorder, which maximize the freedom of movement [20]. Therefore, it is challenging to achieve simultaneously high conductivity and stretchability. In this work, we addressed this challenge by constructing FCAP films with the aid of PEO to achieve a better balance between fantastic conductivity and remarkable mechanical stretchability. To understand the effects of PEO on conductivity and mechanical stretchability, a comprehensive analysis of the structure of FCAP films was conducted. In Raman spectra, the

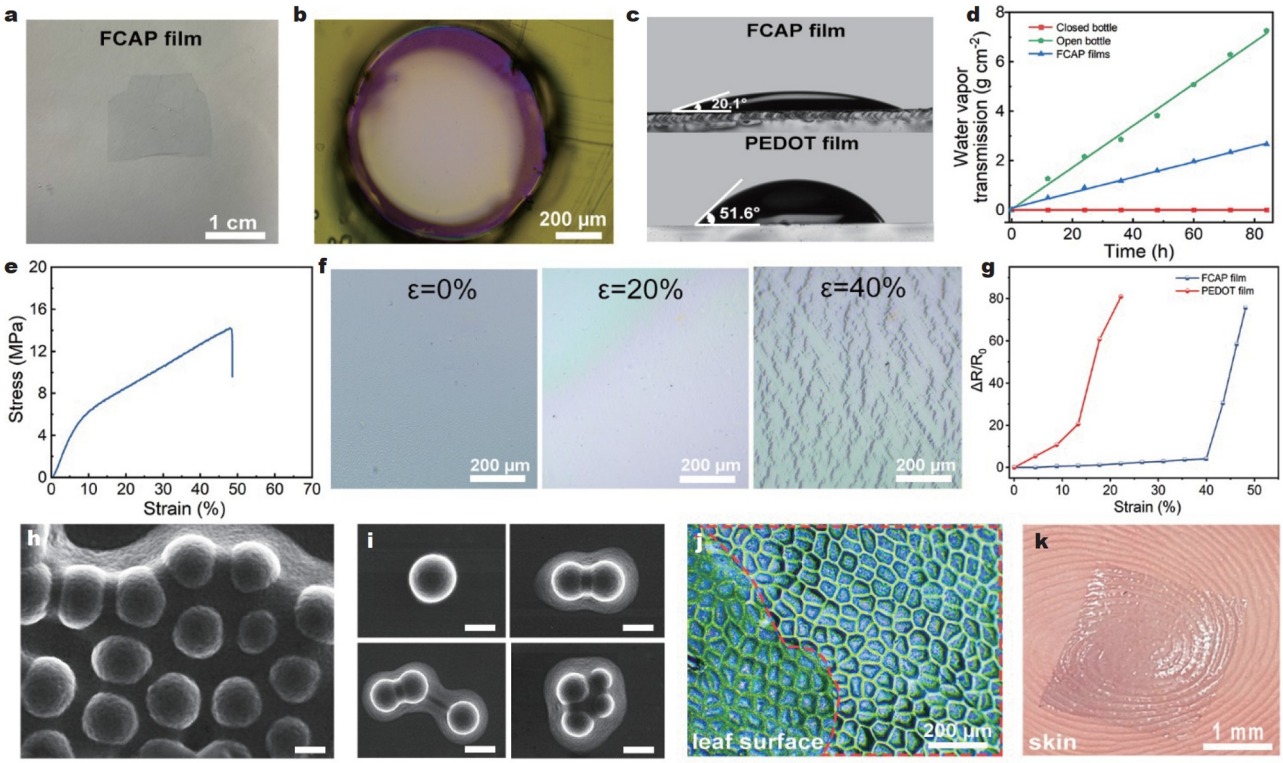

Figure 2 Material characteristics of the FCAP films. (a) Photograph of the FCAP film floating on water. (b) Optical microscope image of the FCAP film suspended over a polyimide substrate with circular holes. (c) Water contact angles of the FCAP film (top) and the PEDOT film (bottom). (d) Water vapor transmission through FCAP films. (e) Stress-strain curve of the FCAP thick film. (f) Optical micrographs of the FCAP films at different tensile strains. (g) Resistance-strain curves of the FCAP films and PEDOT films with PDMS substrates. (h, i) SEM images showing the contact interface between the 10-μm-diameter silica microspheres of different configurations with the FCAP films (scale bars = 4 μm). (j) Optical micrographs of the FCAP film on the surface of a leaf. (k) A micrograph of an FCAP film on the skin of a fingertip.

C_α=C_β stretching vibration on the five-membered rings of PEDOT film located between 1400 and 1500 cm^{-1} is red-shifted and narrowed after doping with PEO (Fig. 3d) [28]. In other words, the resonant structure of the PEDOT chain changed from benzoid to quinoid in the presence of PEO, resulting in a more planar backbone. This planarity may contribute to more efficient charge delocalization and a higher packing order. More detailed information has been investigated as shown in Figs S11 and S12. Cyclic voltammetry (CV) curves further confirm the structural changes of the PEDOT chains (Fig. 3e). It can be seen that the redox behaviors show obvious changes along with doubling the integrated current in FCAP films. This implies that there is a significant increase in conductivity after doping the PEDOT chains, which is due to the conformational change of the PEDOT chains when the irregular poly(3-dodecylthiophene) becomes regular poly(3-dodecylthiophene) [28]. Grazing-incidence wide-angle X-ray scattering (GIWAXS) also confirms that the ordering of semi-crystalline PEDOT films increases significantly with increasing PEO contents (Fig. 3f and Fig. S13). The 1D scattering profiles along the q_z direction are obtained from the 2D GIWAXS patterns. The (010) peak at around q_z = 1.8 $Å^{-1}$ is attributed to the π-π stacking of PEDOT [29]. The π-π stacking peaks are observable from both out-of-plane and in-plane, revealing the fact that the stacking in face-on orientation is approximately similar to that in edge-on orientation. After PEO doping, the crystallinity and orientation of PEDOT have been significantly improved. The enhancement of the weight fraction of PEO to 33 wt% leads to the most obvious crystalline reflections. The clear π-π stacking peaks reveal a more organized arrangement of the PEDOT chains.

Consequently, a schematic diagram (Fig. 3g) was drawn to illustrate how the conductivity and stretchability of FCAP films can be enhanced by the synergy of PEDOT:PSS and PEO. A general model of PEDOT film shows that the PEDOT film consists of grains with a highly conductive hydrophobic PEDOT-rich core and an insulating hydrophilic PSS-rich shell [30]. The PEO molecules with polar groups and high dielectric constants preferentially interact with hydrophilic PSS, resulting in shielding of the PEDOT chains and PSS chains. The shielding effect facilitates the phase separation between PEDOT chains and PSS chains, which enables the reorientation of the PEDOT polymer chains from coiled structures to linear structures, and enhances the inter-chain interactions. As a result, the energy barrier of charge hopping between inter-chains and inter-domains is reduced, and the conductivity of FCAP films is enhanced. Atomic force microscopy (AFM) phase images further support this hypothesis (Fig. 3h–k and Fig. S14). The screening effect of PEO results in a morphological change to form more crystalline and interconnected PEDOT nanofiber structures. The microscopic nanofiber structures of FCAP films are most pronounced when the concentration of PEO was 33 wt%, which confirms the highest electrical conductivity and stretchability compared with the previous films. However, once the weight fraction threshold is exceeded, large crystalline

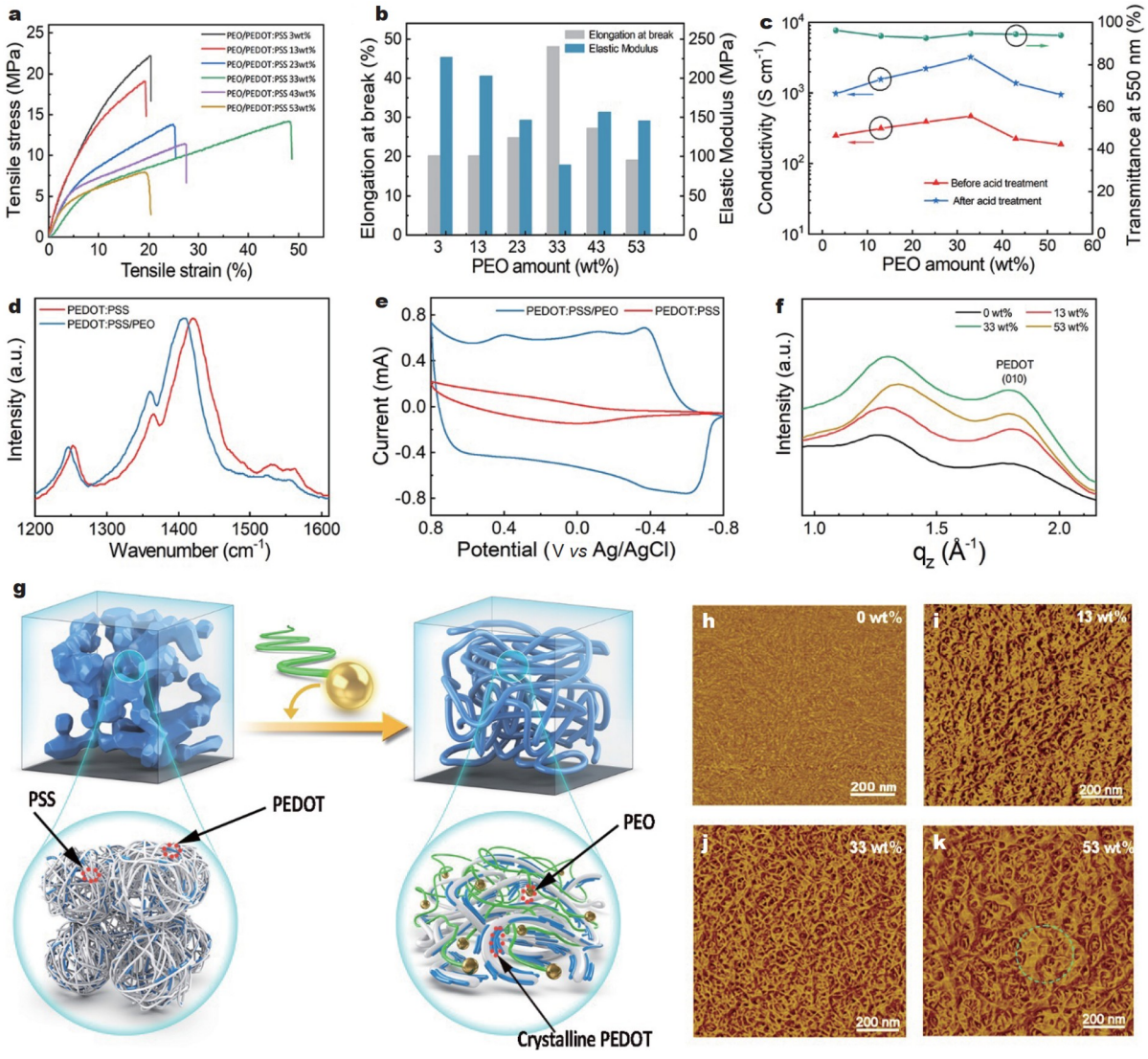

Figure 3 Microstructure characterizations and formation mechanism analysis of FCAP films. (a) Stress-strain behaviors, (b) elongations at break and Young's moduli of the FCAP films with various amounts of PEO. (c) Conductivity and transmittance of the FCAP films. (d) Raman spectra illustrating the C_α=C_β peak position shift in the FCAP films. (e) CVs of the PEDOT films doped with and without PEO. (f) Near out-of-plane intensity plot of the FCAP films. (g) Corresponding schematic depicting phase separation generation in the PEDOT film (white: PSS, blue: PEDOT, and green: PEO). (h–k) AFM phase images of the FCAP films with different amounts of PEO.

particles are formed, resulting in reduced stretchability [31].

Monitoring electrophysiological signals with ASU-EBEs based on FCAP films

The resulting FCAP films are considered to be an optimal choice for the manufacture of epidermal bioelectrodes due to their remarkable mechanical properties, such as high stretchability, ultra-thin free-standing form and reasonable Young's modulus. The construction of ASU-EBEs with FCAP films can be obtained through the "wet transfer" method, as depicted in Fig. 4a. When the skin undergoes various large deformations like stretching, compressing and twisting, the ASU-EBE maintains conformal deformations (Fig. 4a). The attainment of high-quality bioelectric signals is widely acknowledged to rely on decreased interfacial contact impedance, a pivotal parameter for epidermal bioelectrodes. The primary reason for the low interfacial impedance of FCAP film as an ASU-EBE lies in its ultra-conformality and excellent conductivity. This conformability is verified through SEM and optical micrographs of the ASU-EBE on porcine skin (Fig. 4b, c). Consequently, a series of contact impedance tests were conducted to demonstrate the improved capabilities of the bioelectrodes. The assessment of interfacial contact impedance between the electrodes and skin was executed on the human arm with the electrodes placed on the surface (Fig. 4d). In comparison to commercial Ag/AgCl gel electrodes, the contact impedance of the resulting ASU-EBE was approximately 48 kΩ at 100 Hz, which is lower than that of Ag/AgCl electrodes (~87 kΩ).

ECG is one of the most common examination items in daily physical check-ups, playing a crucial role in the early diagnosis of numerous diseases [25]. ECG signals traverse through cardiac tissue, generating distinct PQRST waveforms (Fig. 4e, f). In this study, two square ASU-EBEs were attached on the forearm for measuring ECG signals (Fig. S15). The ASU-EBEs exhibit high-

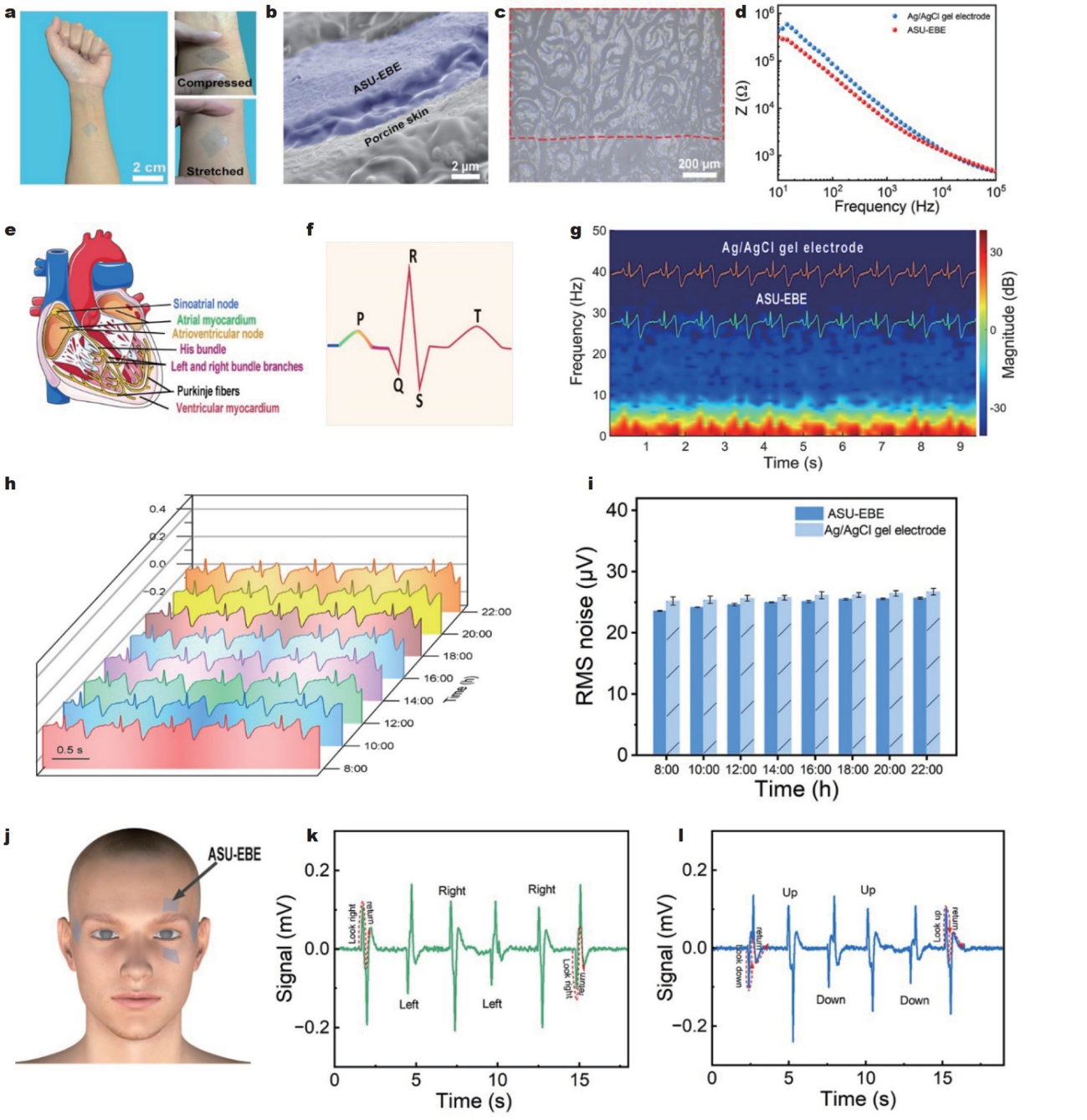

Figure 4 Advanced epidermal bioelectrodes based on the FCAP film for the ECG and EOG detection. (a) The FCAP film was transferred to the arm and was resistant to various mechanical deformations (e.g., stretching and compression). (b, c) A cross-sectional SEM image and optical micrograph of the bioelectrode on porcine skin (bottom). (d) Interfacial contact impedances of ASU-EBE (red) and Ag/AgCl (blue) electrode. (e) Schematic diagram of cardiac tissue structure. (f) ECG of a heart in normal sinus rhythm. (g) ECG signals recording and the corresponding time-frequency spectrograms (yellow: Ag/AgCl electrode, and green: ASU-EBE). (h, i) Long-term monitoring of ECG using ASU-EBE for 1 day and their RMS noise. (j–l) Schematic illustration of electrode placement for EOG and EOG signals corresponding to the differential channel that records left-right and up-down eye movements, respectively.

quality ECG signals with clear PQRST waveforms, compared with that using standard Ag/AgCl gel electrodes (Fig. 4g). Furthermore, the Fourier transform analysis was applied to acquire the spectrogram of the ECG pulses within the 0–50 Hz range, facilitating identification of specific peaks within the PQRST waveform and assessment of signal intensity ranging from 20–40 dB (Fig. 4g and Fig. S16). These parameters hold significant clinical relevance for diagnosing cardiac abnormalities such as congenital heart defects, arrhythmias, or potential heart failure. The ASU-EBE demonstrates remarkable efficacy for long-term healthcare monitoring by consistently delivering high-quality ECG signals even after continuous usage spanning 14 h (Fig. 4h). Furthermore, noise analysis utilizing root-mean-squared (RMS) indicates that the ASU-EBE exhibits lower noise levels compared with Ag/AgCl gel electrodes during prolonged monitoring sessions (Fig. 4i). Collectively, these findings substantiate that ASU-EBEs outperform traditional gel electrodes when it comes to extended duration monitoring of ECG signals.

Furthermore, the ASU-EBEs were attached to the forehead and lower eyelids in order to assess the oculomotor function in a noninvasive manner (Fig. 4j). They were positioned on the sides of the eyes and were differentially connected to a separate channel. When the subject gazes in a specific direction, the resulting cornea-retina depolarization generates electric potential differences associated with the eye movement. Consequently, the EOG signal of the corresponding channel is modified (Fig. 4k). Likewise, when the subject looks up or down, a distinct pattern is recorded by a separate pair of electrodes (Fig. 4l). Different gazing patterns (e.g., up-down, up-center, left-center, and center-right) can be distinguished during slower gazing experiments. The results indicate that the progress of this ASU-EBE has contributed to the development of eye tracking technology in the human-machine interface.

Compared with ECG and EOG recording, long-term reliable EEG monitoring is more difficult because the EEG signal is weak (μV level) and susceptible to external interference. Nevertheless, real-time and high-quality EEG recordings are crucial for clinical and brain science applications [3]. To collect EEG signals from the occipital lobe, two ASU-EBEs were accurately placed at Fp1 and Fp2 locations on the subject's forehead. These electrodes were subsequently sampled individually, with a shared ground electrode attached to the earlobe (Fig. S17a). The volunteer was comfortably seated and exposed to white noise to prevent auditory interference. The potentials of both the open and closed eye were detected. When a person closes his or her eyes, his or her biopotentials show frequencies between 7 and 15 Hz, corresponding to characteristic alpha waves (Fig. S17b). However, the EEG signals exhibit a wider frequency range when the eyes are open. After performing a short-time Fourier transformation (STFT) on the signals, the resulting spectrogram displays a heatmap of the frequency components and power levels (in dB) over the entire time trace (Fig. S17b).

Surface EMG (sEMG), which collects muscle electrical activity from the skin's surface through non-invasive detection, has become common in the field of human-machine interfaces [32]. In this research, the ASU-EBEs served as conductive interfaces between human skin and an electromyograph for collecting sEMG signals (Fig. 5a, d). The resulting ASU-EBEs exhibit high-quality physiological electrical signals compared with commercial Ag/AgCl electrodes (Fig. 5e). The SNR of the sEMG signals recorded by the ASU-EBE is 19.909 dB, higher than that recorded by the Ag/AgCl gel electrodes (12.776 dB). The application of different forces to the grip strength meter enables the monitoring of the gradual increase of sEMG signals (Fig. 5f, g). Furthermore, ASU-EBEs can monitor various activities of the human body at distinct muscle locations (Fig. 5h). The application of sEMG signals on the leg muscles provides the evaluation of knee flexion angle, as depicted in Fig. 5h(i). In

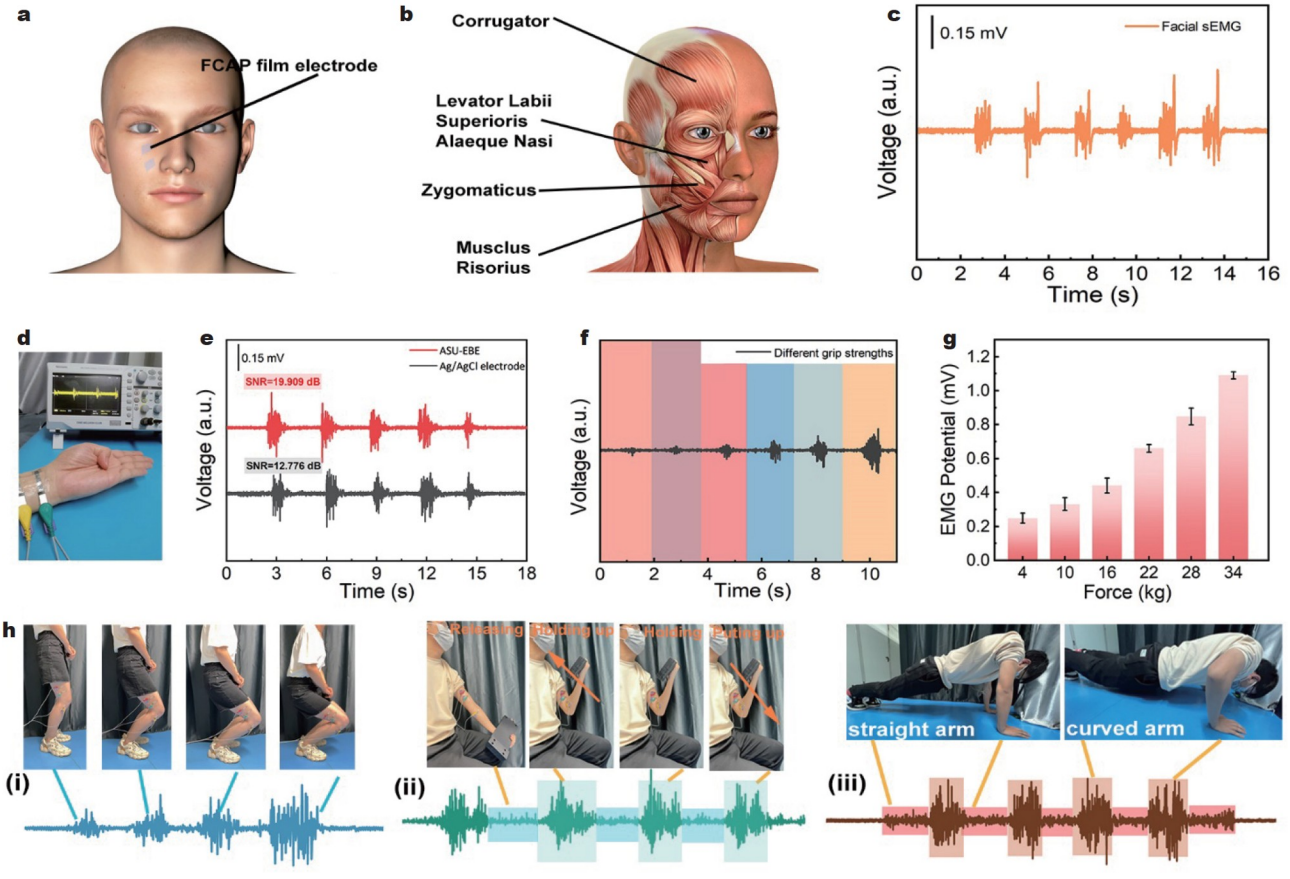

Figure 5 sEMG monitoring of human movements. (a) Schematic of the electrode placement for facial sEMG experiments performed with ASU-EBEs. (b) A photograph of facial expression muscles. (c) Facial sEMG. (d) Picture of sEMG test: ASU-EBEs are attached to the skin near the muscle. (e) Comparision of sEMG signals of that used commercial Ag/AgCl electrodes (black line) and ASU-EBEs (red line). (f) Variation of sEMG signal with grip strength. (g) sEMG measured at varying gripping forces. (h) Detection of body exercises from sEMG signal and the corresponding images (inset), squatting (i), weightlifting (ii), and push-up (iii).

addition, it can distinguish between pushing ups and lifting dumbbells by transferring ASU-EBEs to the arm muscles, generating different sEMG signals (Fig. 5h(ii) and (iii)).

sEMG-robot interaction

Furthermore, the collected sEMG signals can remotely control robots through amplification and programming procedures (Fig. 6a). Different amplitudes of sEMG signals were recorded when individual fingers of the hand were bent with varying intensities (Fig. 6b). Signal processing techniques, including filtering, calibration, and feature extraction, can be employed to process raw sEMG signals, which can subsequently undergo additional processing *via* communication interface devices. To accurately monitor the sEMG signals generated by each finger activity, five pairs of ASU-EBEs were placed at different locations on the arm to collect the signals (Fig. 6a and Fig. S18). The front-end analog circuit collects these sEMG signals, and the back-end digital signal is subsequently filtered and processed (Fig. 6c). Subsequently, the robot's walking route and the manipulator's corresponding finger movements are output *via* the wireless Bluetooth or USB interface (Fig. 6a). Varying finger bends correspond to different sEMG signal strengths, enabling robot control for walking forward, backward, left, or right (Fig. 6d, and Movies S4, S5). Moreover, the sEMG signal facilitates the synchronous movement of human fingers and artificial fingers, providing significant convenience for the daily life of people with motor control disorders (Fig. 6e).

CONCLUSIONS

In conclusion, we present an unprecedented effective strategy for developing substrate-free ultra-thin breathable epidermal bioelectrodes based on FCAP films. This is achieved by incorpor-

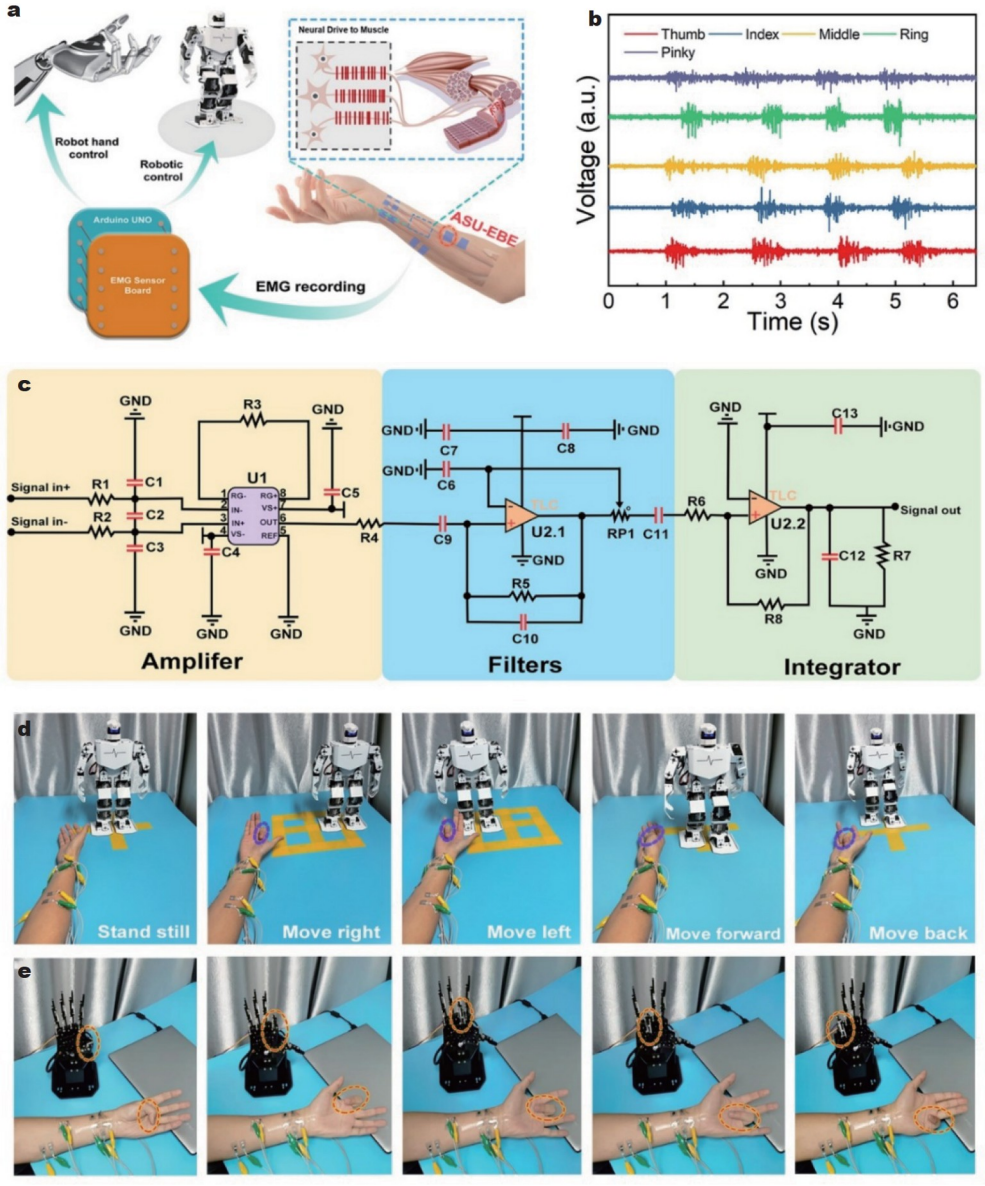

Figure 6 sEMG acquisition and sEMG-robot interaction. (a) Schematic diagram of the acquisition and processing output of sEMG-robot interaction signals. (b) sEMG signals corresponding to different finger movements. (c) Circuit diagrams of sEMG sensor board. (d) sEMG signals are used to control robot movement (move right, left, forward, and back). (e) sEMG signals are used to control mechanical hand movement.

ating the water-soluble polymer PEO into PEDOT:PSS, which combines remarkable stretchability and ultra-conformality. The PEO molecules with polar groups and high dielectric constants induce a shielding effect between PEDOT chains and PSS chains, facilitating the formation of nanofiber structures in FCAP films, which synergistically enhances their electrical conductivity and mechanical stretchability. It has been observed that the resonant structure of the PEDOT chain changed from benzoid to quinoid in the presence of PEO, resulting in a more planar backbone, which contributes to more efficient charge delocalization and higher packing order. Consequently, doping with PEO significantly improves the crystallinity and orientation of PEDOT. Furthermore, the FCAP films exhibit structural robustness and mechanical properties comparable to those of soft biological tissues, thus improving their natural adaptation to microscopic topography. As a result, ASU-EBEs produced based on these FCAP films demonstrate successful recording capabilities for multiple bioelectronic signals including ECG, EOG, EMG, and EEG. This effective signal collection underscores the outstanding practical capabilities of these breathable ASU-EBEs particularly in challenging scenarios.

Received 1 January 2024; accepted 16 February 2024; published online 24 April 2024

1 Zhang M, Tang Z, Liu X, *et al.* Electronic neural interfaces. Nat Electron, 2020, 3: 191–200
2 Wang Y, Haick H, Guo S, *et al.* Skin bioelectronics towards long-term, continuous health monitoring. Chem Soc Rev, 2022, 51: 3759–3793
3 Wang C, Wang H, Wang B, *et al.* On-skin paintable biogel for long-term high-fidelity electroencephalogram recording. Sci Adv, 2022, 8: eabo1396
4 Liu S, Rao Y, Jang H, *et al.* Strategies for body-conformable electronics. Matter, 2022, 5: 1104–1136
5 Zhang L, Kumar KS, He H, *et al.* Fully organic compliant dry electrodes self-adhesive to skin for long-term motion-robust epidermal biopotential monitoring. Nat Commun, 2020, 11: 4683
6 Miyamoto A, Lee S, Cooray NF, *et al.* Inflammation-free, gas-permeable, lightweight, stretchable on-skin electronics with nanomeshes. Nat Nanotech, 2017, 12: 907–913
7 Zhu Y, Haghniaz R, Hartel MC, *et al.* A breathable, passive-cooling, non-inflammatory, and biodegradable aerogel electronic skin for wearable physical-electrophysiological-chemical analysis. Adv Mater, 2023, 35: 2209300
8 Someya T, Amagai M. Toward a new generation of smart skins. Nat Biotechnol, 2019, 37: 382–388
9 Zhao Y, Zhang S, Yu T, *et al.* Ultra-conformal skin electrodes with synergistically enhanced conductivity for long-time and low-motion artifact epidermal electrophysiology. Nat Commun, 2021, 12: 4880
10 Fernandez M, Pallas-Areny R. Ag-AgCl electrode noise in high-resolution ECG measurements. Biomed Instrum Technol, 2000, 34: 125–130
11 Deng J, Yuk H, Wu J, *et al.* Electrical bioadhesive interface for bioelectronics. Nat Mater, 2021, 20: 229–236
12 Gogurla N, Kim Y, Cho S, *et al.* Multifunctional and ultrathin electronic tattoo for on-skin diagnostic and therapeutic applications. Adv Mater, 2021, 33: 2008308
13 Kabiri Ameri S, Ho R, Jang H, *et al.* Graphene electronic tattoo sensors. ACS Nano, 2017, 11: 7634–7641
14 Tang L, Shang J, Jiang X. Multilayered electronic transfer tattoo that can enable the crease amplification effect. Sci Adv, 2021, 7: eabe3778
15 Jiang Z, Chen N, Yi Z, *et al.* A 1.3-micrometre-thick elastic conductor for seamless on-skin and implantable sensors. Nat Electron, 2022, 5: 784–793
16 Kireev D, Sel K, Ibrahim B, *et al.* Continuous cuffless monitoring of arterial blood pressure *via* graphene bioimpedance tattoos. Nat Nanotechnol, 2022, 17: 864–870
17 Jang H, Sel K, Kim E, *et al.* Graphene e-tattoos for unobstructive ambulatory electrodermal activity sensing on the palm enabled by heterogeneous serpentine ribbons. Nat Commun, 2022, 13: 6604
18 Song D, Ye G, Zhao Y, *et al.* An all-in-one, bioderived, air-permeable, and sweat-stable MXene epidermal electrode for muscle theranostics. ACS Nano, 2022, 16: 17168–17178
19 Yan Z, Xu D, Lin Z, *et al.* Highly stretchable van der Waals thin films for adaptable and breathable electronic membranes. Science, 2022, 375: 852–859
20 Wang Y, Zhu C, Pfattner R, *et al.* A highly stretchable, transparent, and conductive polymer. Sci Adv, 2017, 3: e1602076
21 Fan X, Nie W, Tsai H, *et al.* PEDOT:PSS for flexible and stretchable electronics: Modifications, strategies, and applications. Adv Sci, 2019, 6: 1900813
22 Ju D, Kim D, Yook H, *et al.* Controlling electrostatic interaction in PEDOT:PSS to overcome thermoelectric tradeoff relation. Adv Funct Mater, 2019, 29: 1905590
23 Jiang Y, Zhang Z, Wang YX, *et al.* Topological supramolecular network enabled high-conductivity, stretchable organic bioelectronics. Science, 2022, 375: 1411–1417
24 Kottner J, Lichterfeld A, Blume-Peytavi U. Transepidermal water loss in young and aged healthy humans: A systematic review and meta-analysis. Arch Dermatol Res, 2013, 305: 315–323
25 Hong YJ, Jeong H, Cho KW, *et al.* Wearable and implantable devices for cardiovascular healthcare: From monitoring to therapy based on flexible and stretchable electronics. Adv Funct Mater, 2019, 29: 1808247
26 Kireev D, Okogbue E, Jayanth RT, *et al.* Multipurpose and reusable ultrathin electronic tattoos based on $PtSe_2$ and $PtTe_2$. ACS Nano, 2021, 15: 2800–2811
27 Salatino JW, Ludwig KA, Kozai TDY, *et al.* Glial responses to implanted electrodes in the brain. Nat Biomed Eng, 2017, 1: 862–877
28 Ouyang J, Xu Q, Chu CW, *et al.* On the mechanism of conductivity enhancement in poly(3,4-ethylenedioxythiophene):poly(styrene sulfonate) film through solvent treatment. Polymer, 2004, 45: 8443–8450
29 Kee S, Kim N, Kim BS, *et al.* Controlling molecular ordering in aqueous conducting polymers using ionic liquids. Adv Mater, 2016, 28: 8625–8631
30 Kayser LV, Lipomi DJ. Stretchable conductive polymers and composites based on PEDOT and PEDOT:PSS. Adv Mater, 2019, 31: 1806133
31 Li P, Sun K, Ouyang J. Stretchable and conductive polymer films prepared by solution blending. ACS Appl Mater Interfaces, 2015, 7: 18415–18423
32 Roberts T, De Graaf JB, Nicol C, *et al.* Flexible inkjet-printed multi-electrode arrays for neuromuscular cartography. Adv Healthcare Mater, 2016, 5: 1462–1470

Acknowledgements This work was supported by the National Key Research and Development Program of China (2023YFB3608904), the National Natural Science Foundation of China (21835003 and 61704077), the Natural Science Foundation of Jiangsu Province (BE2019120 and BK20191374), the Foundation of Key Laboratory of Flexible Electronics of Zhejiang Province (2023FE002), the Natural Science Foundation of Jiangsu Higher Education Institutions of China (18KJB150025), the Program for Jiangsu Specially-Appointed Professor (RK030STP15001), the Postgraduate Research & Practice Innovation Program of Jiangsu Province (KYCX21_0778, SJCX21_0298), the NUPT Scientific Foundation (NY219021 and NY219109), the Leading Talent of Technological Innovation of National Ten-Thousands Talents Program of China, and the Priority Academic Program Development of Jiangsu Higher Education Institutions (PAPD).

Author contributions Niu J and Lai WY conceived the idea; Li G carried out the material synthesis and performed the material characterization; Fang S, Gong Y, Shao R, and You T contributed to the electrophysiological measurement and design of human-machine interaction programs; Li G, Gong Y, Niu J, and Lai WY co-wrote the paper. All authors discussed the results and commented on the manuscript.

Conflict of interest The authors declare that they have no conflict of interest.

Supplementary information Experimental details and supporting data are available in the online version of the paper.

Guanjun Li is a PhD candidate at Nanjing Post and Communications University. His research focuses on the development of high-performance electronic skins and epidermal electronics, including adhesive bioelectronic materials and devices, new conductive hydrogels, and biological tissue-electrode interface sensing technology.

Jian Niu is an associate professor at Nanjing University of Posts and Telecommunications. He received his PhD in physics from Lanzhou University in 2011. His research primarily focuses on the development and application of flexible and stretchable electronic devices.

Wen-Yong Lai is a full professor at Nanjing University of Posts and Telecommunications. He received his PhD degree from Fudan University in 2007. He then joined the Key Laboratory for Organic Electronics & Information Displays, Institute of Advanced Materials (IAM), Nanjing University of Posts and Telecommunications. His research mainly focuses on the design, synthesis, and application of organic & polymer optoelectronic materials for organic/flexible electronics. He is also interested in the exploration of novel materials and processes for printed electronics.

具有增强一致性和透气性的无基底超薄表皮生物电极用于长期生理监测

李冠军[†], 公彦婷[†], 方诗锶, 游通, 邵瑞瑞, 姚兰前, 刘晨, 武春锦, 牛坚[*], 赖文勇[*]

摘要 开发耐用且可靠的生物电极, 用以采集高质量的生物电信号, 已成为人体生理状态监测和人机交互领域的关键技术. 然而, 现有的生物电极多基于传统弹性基底, 这导致了机械性能不匹配和低渗透性等问题, 并且缺乏与生物皮肤类似的多方面属性和必要的协同特性. 本研究中, 我们报道了一种新型的基于自支撑导电全聚合物薄膜的超薄表皮生物电极(ASU-EBE). 该电极将超一致性、优异的拉伸性和透气性集成于一体, 展现了约475 S cm^{-1}的高导电性, 约48%的出色拉伸性, 与生物组织界面的超一致性以及优异的透气性. 该电极的电子和机械性能得到提升, 这归功于在PEDOT:PSS中引入水溶性聚氧化乙烯, 以调节分子间π-π堆积距离, 并促进纳米纤维结构的形成. 因此, ASU-EBE在与皮肤接触时的阻抗远低于标准凝胶电极, 使其成为复杂日常环境下长期医疗监测的理想选择.

